Bulletin of the Seismological Society of America, 91, 3, pp. 538–552, June 2001

Failure, Memory, and Cyclic Fault Movement

by Kagan Tuncay, A. Khalil, and Peter J. Ortoleva

Abstract Faulting is typically a two timescale process, that is, rapid failure and slow (chemical) healing. Once failed, a rock has a long memory until slow chemical processes have time to re-establish the grain–grain contacts underlying rock competency. The memory of rock failure can be captured by a sufficiently rich textural model, and the texture must be coevolved with rock stress and deformation to yield a self-consistent model of strain hardening/weakening, fault narrowing, and earthquake cyclicity.

A model based on incremental stress rheology and rock texture dynamics is introduced that emphasizes the interplay of rock competency, porosity, and other texture variables with stress and strain. The deformation mechanisms taken into consideration are poroelasticity and viscosity. The rheology equations are strongly coupled to the evolution equations of rock texture and pore fluid flow.

The model is used to gain an understanding of several oscillatory modes of fault movement. The roles of rock competency, fluid pressure, and continuous deformation in these oscillations is illustrated for various conditions. The approach is shown to be a natural starting point for a theory of the three-dimensional, multiprocess dynamics of fault nucleation, growth, morphology, reactivation, and continuous versus seismic behavior.

Introduction

The objective of this study is to demonstrate how fault dynamics may naturally be placed in the context of incremental stress theory, rock textural evolution modeling, and standard conservation laws. Casting the fault dynamics problem in this framework naturally introduces rock memory for failure, fluid pressure effects, and the autonomous nature of earthquake cyclicity.

The deformation of brittle rocks is a multiple time and length scale phenomenon. Rocks fail rapidly but heal slowly on geological time scales (Fredrich and Evans, 1992; Logan and Teufel, 1986). Brittle rocks have two sources of memory. They store elastic energy, and, once failed, have broken grain–grain contacts and gouges that persist over long times. Viscous deformation or failure erase the former, whereas chemical healing processes diminish or erase the latter. When sheared across a large-scale zone, they can fail within a meter-scale fault zone. Furthermore, the fault dynamic typically takes the form of a series of short time-scale events with long interevent healing periods to form the earthquake cycle. The challenge is to develop a rheologic model of this deformation behavior that captures this multiple scale character autonomously, that is, from an initially uniform, unfailed system to a faulted one experiencing intermittent failure-healing cyclicity and complex spatial structure.

Interest in slip instability has increased considerably since Brace and Byerlee (1966) proposed that it might be related to earthquake rupture (see Scholz [1992], for an historical review). Research on the slip instability is mostly based on experiments (Dieterich, 1978, 1979; Tullis, 1988; Blanpied *et al.,* 1995; Linker and Dieterich, 1992) that show that the rate dependent friction coefficient is a result of two competing processes. As slip velocity is changed, an almost instantaneous change in friction coefficient is observed. This sudden change in friction coefficient is followed by a gradual evolution period. The friction coefficient is usually assumed to be a function of slip velocity and a number of state variables governed by ordinary differential equations (Dieterich, 1979; Rice and Gu, 1983; Ruina, 1983; Rice and Ruina, 1983; Tse and Rice, 1986). Recent advances include the dependence of the friction coefficient on normal stress (Linker and Dieterich, 1992; Sleep, 1997), temperature (Chester 1994; Sleep, 1995b, 1997), and wetting (Chester, 1995).

The rate- and state-dependent friction models introduce a number of state variables that are governed by ordinary differential equations (Dieterich, 1979; Rice and Gu, 1983; Ruina, 1983; Rice and Ruina, 1983; Tse and Rice, 1986). The physical interpretations of these state variables are often ambiguous. A more general approach is the use of texture variables such as grain size distribution, porosity, and packing as the state variables of the system. The key to this approach is that the memory of rocks is to be captured by a sufficiently rich textural model and that the texture must be

coevolved with rock stress and deformation to yield a self-consistent model of strain hardening/weakening, fault narrowing, and earthquake cyclicity. In the present study, these multiple scale and autonomous fault behaviors are shown to follow naturally from the feedback between stress and rock texture as suggested in Figure 1. Rock deformation is thereby autonomous—stress changes texture, texture changes rock rheology, and, in turn, rock rheology affects stress. This feedback is shown here to be more self-consistent and fundamental than concepts such as strain hardening/weakening or velocity-dependent viscosity.

We suggest that rigorous models of rock behavior should be of the Markov type, that is, the rate of change of rock state should only depend on the instantaneous rock state and not on prior history. Stress and strain are related through rock rheology, to rock texture Θ (a set of variables including grain size, shape, packing, and mineralogy). Pressure solution and grain breakage imply that the rate of change of Θ depends on stress, denoted σ. If Θ satisfies

$$\frac{d\Theta}{dt} = G(\Theta, \sigma), \tag{1}$$

then, in principle, $\Theta(t)$ is a functional of σ, that is, it depends on $\sigma(t')$ for all $t' < t$, namely, on the stress history: $\Theta = \Theta[\sigma]$. As rheology depends on Θ, we see that $\Theta[\sigma]$ reflects the entire prior stress history and not just the instantaneous value of σ. Clearly, however, this memory in a theory wherein Θ is not coevolved with σ is an artifact of the incompleteness of a rock deformation model that attempts to avoid coevolving Θ with stress. While there are many stress-strain histories that could lead to the instantaneous state of a rock, only the latter is key to predicting its failure and other behavior.

Thus, strain hardening/weakening does not seem to be a viable starting point for a predictive model. Rather, we propose a Markov approach wherein texture, stress and other variables are coevolved. In our earlier work we have shown that a model of the Markov type, wherein texture is coevolving with deformation, can capture phenomena such as metamorphic layering, self-organized diagenetic layering, stylolites, flow/fracturing temporal cycles, and self-organized compartments (see Ortoleva, 1990, 1994a,b, 1998; Dewers and Ortoleva, 1995; Tuncay *et al.,* 2000a,b; Ozkama and Ortoleva, 2000; Renard and Ortoleva, 2001, for reviews and citations). In this way, earthquake cyclicity, like these other self-organized phenomena, are given the unifying perspective of the theory of nonlinear dynamical systems. They autonomously arise from the network of reaction, transport, and mechanical (RTM) crustal processes; there spatiotemporal pattern is not imposed from outside the system.

As geologic evidence is gathered on the involvement of fluids in faults, a growing number of researchers has started to study the effect of fluid pressure on fault mechanics (Lachenbruch, 1980; Sleep and Blanpied, 1994; Chester,

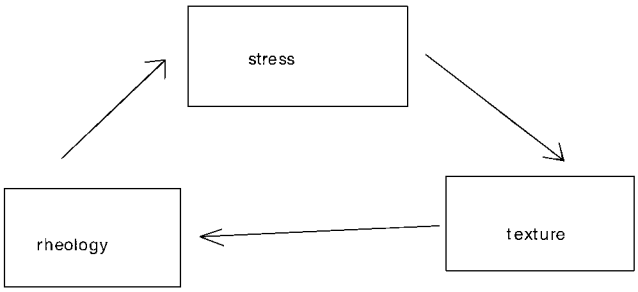

Figure 1. Rock deformation feedback.

1995; Hickman *et al.,* 1995; Lockner and Byerlee, 1995; Segall and Rice, 1995; Sleep 1995a, 1997; Fournier, 1996; Lee, 1996; Miller *et al.,* 1996; Henderson and Maillot, 1997; Yamashita, 1997, 1998). Rice (1992) and Byerlee (1990) suggested that relative weakness of some faults could be due to high intrafault fluid pressure. Rice (1992) proposed that overpressuring could be maintained by the flow of deep fluids into the ductile roots of a fault zone. On the other hand, Byerlee's (1990) model explains high overpressure by conjecturing efficiently sealed compartments. Recently, Lee (1996) demonstrated that a sudden temperature increase because of slip friction can also cause significant overpressuring. The concept of compartment abnormal pressuring has been analyzed extensively in the context of sedimentary basins (see Ortoleva 1994b, 1998, and references cited therein).

In an attempt at modeling fluid flow in partially sealed fault zones, Sleep and Blanpied (1994) assumed purely viscous rock behavior. The shear and bulk viscosities were assumed to be functions of the pore and fracture volume fractions that were taken to evolve via two empirical ordinary differential equations. The pressure equation was based on the conservation of fluid phase and included both increase in pressure because of compaction and decrease in pressure due to escape of fluid. In the case of a single fault system, Sleep and Blanpied (1994) showed that the increased fluid pressure allows frictional failure in earthquakes at shear tractions far below those required when fluid pressure is hydrostatic. However, in their numerical treatment, a predetermined shear traction drop was imposed (a fraction of its value), and the displacement, pore volume, and fluid pressure were reset. In other words, in the case of a single-fault system, an oscillation was imposed, not simulated. In a later study, Sleep (1995a) included the changes in temperature (due to frictional heating), effective normal traction, and fault width in the calculations.

Segall and Rice (1995) modified the rate- and state-dependent friction model to include fluid pressure and porosity (based on porosity changes observed in gouge experiments with overcompacted rocks). Their final set of equations includes an ordinary differential equation for velocity-dependent porosity based on experimental observations. In gouge experiments (for overcompacted rocks), if

the normal stress is kept constant, an increase in porosity is observed. The increase in pore volume results in a decrease in fluid pressure and an increase in normal stress, which, in turn, tends to stabilize faulting (also called dilatancy hardening, see Rice [1975]; Rudnicki and Chen [1988]). Similar conclusions were reached by Lockner and Byerlee (1995), who used a series of blocks and springs to represent the fault. Henderson and Maillot (1997) used an empirical exponential function for the reduction of porosity due to compaction. They assumed that in the case of rupture, porosity can increase up to 10%. Miller *et al.* (1996) presented an instability model driven by a porosity reduction mechanism assuming that the fault normal compression compacts the fault zone and reduces the porosity, resulting in high-fluid-pressured compartments. As this short literature survey reveals, although considerable research effort has been spent on the interplay of fluid flow, friction, and failure in the last decade, there is a large number of uncertainties to be resolved in order to identify the dominant mechanism of earthquake cyclicity or to predict fault structure and temporal evolution.

In this study, we consider poroelastic and viscous incremental stress rheology. The evolving texture is represented by the porosity and rock competency. The fraction of grain surfaces shared with other grains is used as a measure of the latter. A Drucker–Prager type criterion is used to signal failure. Rock cohesion is assumed to depend strongly on rock competency, capturing the transition between intact and cohesionless rock. The permeability and shear viscosity are modeled as strong functions of rock competency and porosity. We consider a lumped model of a fault zone interacting with country rock. In a more complete analysis, the equations presented here apply to each finite element in a continuous theory. Because our model is based on rheological laws, force balance, and mass conservation, it can be directly incorporated in a three-dimensional crustal RTM model (see Ortoleva 1994a, 1998; Tuncay, *et al.,* 2000a,b; Tuncay and Ortoleva, 2001). One of the goals of the present work is to develop an intact to failure, comprehensive model so this three-dimensional analysis can lead to a predictive model of fault inner structure, morphology, and complex spatiotemporal dynamics.

Incremental Stress Rheology and Rock Competency

Incremental Stress Rheology

The strongly coupled nature of the crustal deformation problem can be captured using an incremental stress rheology. The specific rheology used in our modeling integrates most of the strain mechanisms believed to operate in the crust. It has the form (Tuncay, Park, and Ortoleva 2000a,b; Ortoleva 1994a, 1998; Ortoleva *et al.* 1997)

$$\dot{\boldsymbol{\varepsilon}} = \dot{\boldsymbol{\varepsilon}}^{\mathrm{el}} + \dot{\boldsymbol{\varepsilon}}^{\mathrm{vp}} + \dot{\boldsymbol{\varepsilon}}^{\mathrm{ps}} + \dot{\boldsymbol{\varepsilon}}^{\mathrm{fr}} + \dot{\boldsymbol{\varepsilon}}^{\mathrm{go}}. \tag{2}$$

Here, $\dot{\boldsymbol{\varepsilon}}$ is the net rate of strain while the terms on the right give the contributions of five processes: poroelasticity (el), continuous viscoplastic (vp), pressure solution (ps), fracturing (fr), and gouge (go). Specific expressions for each term have been taken from the literature. In this study we consider poroelasticity and continuous viscoplasticity.

The poroelasticity rate of strain $\dot{\boldsymbol{\varepsilon}}^{\mathrm{el}}$ may be expressed in terms of stress $\boldsymbol{\sigma}$, pressure p of the (assumed single) fluid phase, and rock texture Θ via

$$\dot{\boldsymbol{\varepsilon}}^{\mathrm{el}} = \mathbf{C}^{-1}(\Theta)\,\frac{D}{Dt}\,(\boldsymbol{\sigma} + \alpha(\Theta)p\mathbf{I}) \tag{3}$$

where $\mathbf{C}$ is the fourth-rank tensor of poroelastic coefficients, α is the effective stress coefficient, and $\mathbf{I}$ is the second-rank identity matrix. Here, D/Dt represents a material time derivative measuring the rate of change of a tensor in time with respect to a local reference frame fixed to a translating, rotating material volume element. The texture Θ represents a set of variables characterizing the mineralogy, shape, size, orientation, and packing of the grains of each mineral. The bulk and shear moduli of the drained porous medium and the effective stress coefficient of the medium can be computed in terms of the Θ and mineral elastic properties using Berryman's (1980, 1986) approach.

The inelastic mechanical contribution to $\dot{\boldsymbol{\varepsilon}}$ is cast in the present approach as a nonlinear viscosity law in the form

$$\dot{\boldsymbol{\varepsilon}}^{\mathrm{vp}} = \boldsymbol{\eta}^{-1}\,(\boldsymbol{\sigma} + \tilde{\alpha}p\mathbf{I}). \tag{4}$$

The fourth-rank viscosity tensor $\boldsymbol{\eta}$ depends on stress, fluid pressure, and texture. The second term in the effective stress involves a coefficient $\tilde{\alpha}$ that is usually taken in the literature to be unity. The shear viscosity is assumed to be a strong function of rock competency (discussed subsequent). Sleep and Blanpied (1994) assumed that the viscosities depend on the intrinsic viscosity of grains and the volume fractions of pores and fractures. However, they did not consider the sudden drop in the shear viscosity due to failure, which is one of the key parameters required to model the stress drop following rupture. We expect that in the case of failure, the change in the shear viscosity is greater than the change in the bulk viscosity. Since the state of stress is strongly dependent on the viscosity ratio, this feedback might play an important role in the reorganization of fault zones after failure.

The texture must be further augmented when rock competency is considered. This is described in the Rock Competency section. Again, in the spirit of our Markov approach, it is only when Θ is sufficiently comprehensive can a self-consistent deformation model be set forth. One expects that $\dot{\boldsymbol{\varepsilon}}^{(j)}$, j = poroelasticity, viscosity, pressure solution, fracturing, gouge, and so forth, should depend on all the aforementioned variables ($\boldsymbol{\sigma}$, Θ, p, c, T). With this,

$$\dot{\boldsymbol{\varepsilon}} = \sum_{j=1}^{N_d} \dot{\boldsymbol{\varepsilon}}^{(j)} (\Theta, \boldsymbol{\sigma}, p, c, T) \quad (5)$$

for a system with N_d deformation mechanisms. The dependence of the strain rates on state clarifies the central role of incremental stress theory in integrating all the crustal RTM processes into a unified model. It is the coupling allowed by this integration that underlies fault dynamics.

The total rate of strain $\dot{\boldsymbol{\varepsilon}}$ is defined as

$$\dot{\varepsilon}_{ii'} = \frac{1}{2}\left(\frac{\partial u_i}{\partial x_{i'}} + \frac{\partial u_{i'}}{\partial x_i}\right). \quad (6)$$

for rock deformation velocity $\mathbf{u}$ and Cartesian coordinates x_1, x_2, x_3. The six independent components of the symmetric second rank tensor equation (2) must be supplemented with three additional equations so that the three deformation velocity components ($\mathbf{u} = u_1, u_2, u_3$) and the six independent stress components can be determined. The required condition arises from force balance:

$$\sum_{i'=1}^{3} \frac{\partial \sigma_{ii'}}{\partial x_{i'}} + f_i = 0 \quad (7)$$

for body force, f_i, which is given by

$$f_i = g\rho_m \delta_{i3}. \quad (8)$$

Here g is the gravitational acceleration, ρ_m is the crustal mass density, and the 3-direction is upward.

In addition to the coupling of deformation to other phenomena through the incremental stress rheology, there are numerous indirect couplings. For example, rock properties such as permeability, multiphase flow parameters, reactive grain surface area, and thermal conductivity depend strongly on texture. As the latter is affected by stress and deformation, a complex network of coupling relations is thereby expressed. For further discussion of the consequences of this network, see Ortoleva (1994a,b; 1998), Tuncay *et al.* (2000a,b), and Dewers and Ortoleva (1994).

Rock Competency

To predict faulting and other rock failure phenomena, we introduce a model that accounts for rock competency. Let rock competency, Γ, measure the fraction of grain surface that is attached to other grains. Thus Γ is in the range $0 \le \Gamma \le 1$. Large Γ implies competency, whereas in a low Γ rock there are few intact grain–grain contacts. Thus rheologic quantities such as rock strength or viscosity are strongly dependent on Γ.

Schematically, our model is as follows. The equation of motion of Γ is taken in the form

$$\frac{D\Gamma}{Dt} = R(\Gamma, F), \quad (9)$$

where F is a failure function that depends on macroscopic stress, fluid pressure, rock texture, mineralogy, and temperature. In three dimensions, the failure function is assumed to take the form (Drucker and Prager, 1952)

$$F = aJ_1 + \sqrt{J_2} - b \quad (10)$$

where J_1 is the first invariant of the effective stress tensor and J_2 is the second invariant of the deviatoric effective stress tensor. The coefficients a and b can be expressed in terms of angle of internal friction φ and cohesion C determined from conventional triaxial compression experiments (Desai and Siriwardane, 1984)

$$a = \frac{2 \sin \varphi}{\sqrt{3}(3 - \sin \varphi)} \quad (11)$$

$$b = \frac{6C \cos \varphi}{\sqrt{3}(3 - \sin \varphi)}. \quad (12)$$

Here, we assume that cohesion depends on rock competency. For an intact rock ($\Gamma = 1$), b is large. As the rock competency is lost, the cohesion-like term b vanishes. Therefore b is a strong function of Γ taken here to be $b = b^*\Gamma^n$, where b^* refers to the value when $\Gamma = 1$ and n is a phenomenological exponent.

If the dynamics of Γ is relatively fast, its evolution is closely related to the shape of the curve $R(\Gamma, F) = 0$ (see chapters 2 and 3 of Ortoleva [1992] for further discussion). The Γ dynamics is, in a sense, a cooperative phenomenon, that is, a decrease in competence fosters more rapid Γ decline. This is captured by the qualitative picture of Figure 2. A schematic evolution path in the F, Γ plane is shown.

Through this model, failure is rapid, whereas healing can be a much slower process. This follows if R is relatively small when Γ is small and F is less than a healing value F_h. This type of effect gives geological materials the memory they have of zones of earlier faulting. Here, $R(\Gamma, F)$ is taken in the form

$$R(\Gamma, F) = k(\Gamma, F)\left(-F + d_3\left(\frac{1}{2} - \Gamma\right) + \frac{d_2}{\Gamma} + \frac{d_1}{1 - \Gamma} + d_4\right)\Gamma(1 - \Gamma) \quad (13)$$

where d_1, d_2, d_3, and d_4 are material constants. The function k is chosen such that when Γ is small and $F < F_h$, k is small, insuring that healing is slow. Finally, F_h can be determined in terms of d_1, d_2, d_3, and d_4. Conceptually, these parameters depend on mineralogy, grain size, shape, and packing.

Rock Competency: Shear Stress

We now show that the feedback associated with the coupling of shear stress (via incremental stress rheology) and

rock competency naturally supports autonomous oscillation. Consider a simple shear system with the total rate of strain given by the sum of poroelastic and nonlinear viscous contributions. The rate of strain due to poroelasticity can be written in terms of the total rate of strain and rate of strain due to viscosity as $\dot{\boldsymbol{\varepsilon}}^{\mathrm{el}} = \dot{\boldsymbol{\varepsilon}} - \dot{\boldsymbol{\varepsilon}}^{\mathrm{vp}}$. Assuming isotropic simple shear, the following ordinary differential equation for the shear stress is written:

$$\frac{D\tau}{Dt} = \frac{G_f}{\mu(\Gamma)} (2\dot{\varepsilon}\mu(\Gamma) - \tau) \tag{14}$$

where τ, $\dot{\varepsilon}$, G_f, and μ are the shear stress, total rate of shear strain, elastic shear modulus, and shear viscosity, respectively. Shear viscosity is taken to be an increasing function of rock competency $\mu = \mu^*\Gamma^m$. The exponent m is taken as 8 to capture the large change in the order of magnitude of shear viscosity between intact and failed rock. For simplicity, assume that the failure function is in the form $F = |\tau| - c$. In this case, c is taken to be $c = -a(\sigma_n + p) + b^*\Gamma$, where σ_n and p are the normal stress (positive in tension) and fluid pressure, respectively. The coefficient b^* is taken to be 50 MPa within the range of typical rock properties. Note that for small values of Γ, $F \sim |\tau| + a(\sigma_n + p)$ capturing the usual friction law. The term $-a(\sigma_n + p)$ is taken as 30 MPa. The rate of shear strain is either taken to be a specified function of time or determined by the energy dissipation condition

$$\tau\dot{\varepsilon} = \dot{E}, \tag{15}$$

where $\dot{E}$ is the rate of energy input.

Equations (9) and (14) form a strongly coupled set of nonlinear ordinary differential equations for the shear stress and rock competency that were integrated numerically by the fourth-order Runga–Kutta technique with adaptive time stepping. Setting the right-hand side (14) to zero yields for constant $\dot{E}$ and the Druker–Prager failure function (10)

$$\Gamma = \left(\frac{(F + c)^2}{2\mu^*\dot{E}}\right)^{1/m}. \tag{16}$$

Figure 3 illustrates the null curves for different values of $\dot{E}$. For small $\dot{E}$ the stress null curve (16) intersects the S-shape null curve $R = 0$ on the upper stable branch near $\Gamma = 1$ (competent rock), that is, the competent rock viscosity μ^* is sufficiently low that the rate of energy input is equal to the rate of viscous energy dissipation (ductile flow). For very large $\dot{E}$, rock fails but the null curves intersect at the lower stable branch, that is, the rock remains failed because of the very low shear viscosity needed to dissipate the required energy (aseismic faults). For intermediate values of $\dot{E}$, the null curves intersect at the unstable branch of $R = 0$. In this case, for a constant $\dot{E}$, rock fails and heals cyclicly (seismic faults). It is also possible that the null curves intersect at

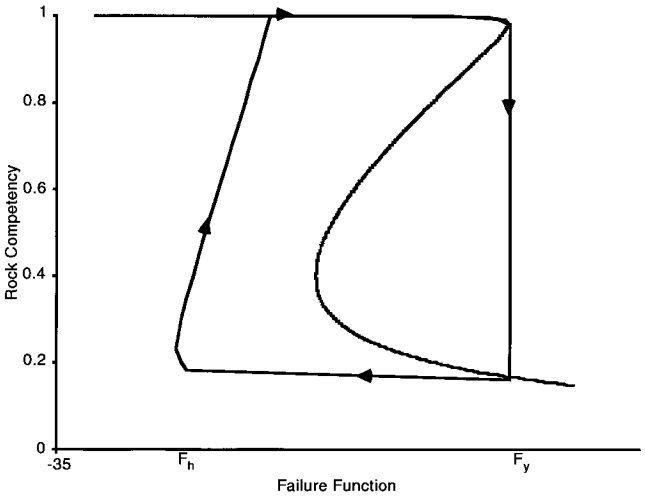

Figure 2. Schematic competence (Γ) and failure function (F) plane illustrating the cooperative aspects of rock failure. When Γ is near unity, the rock is competent, but when F exceeds F_{yield}, it is compromised. However, for $F < F_h$, competence is regained through chemical healing processes. If a point is on the right of the S-shape curve, rock competency decreases otherview it increases.

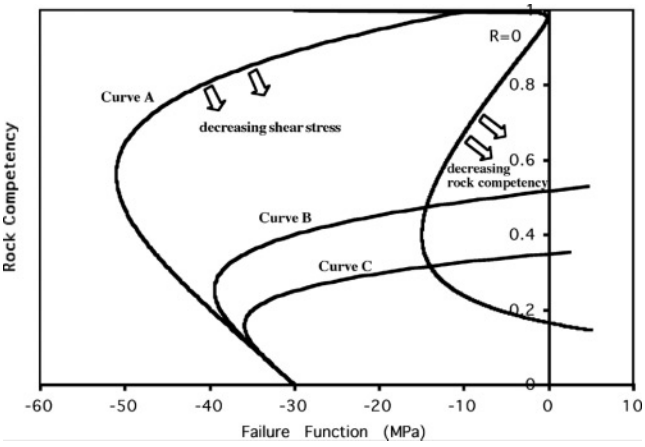

Figure 3. The null curves for equations (11) and (17) for different values of $\dot{E}$ and phase diagram for a variable $\dot{E}$ (Curve A, $\dot{E} = 0.0005$ GPa/m.y.; Curve B, $\dot{E} = 0.06$ GPa/m.y.; Curve C, $\dot{E} = 1$ GPa/m.y.). For very large $\dot{E}$, rock fails but the null curves intersect at the lower stable branch, that is, the rock remains failed because of the very low shear viscosity needed to dissipate the required energy (aseismic faults). For intermediate values of $\dot{E}$, the null curves intersect at the unstable branch of $R = 0$. In this case, for a constant $\dot{E}$, rock fails and heals cyclicly (seismic faults).

three distinct points. In this case, depending on the initial conditions of shear stress and rock competency, rock will either never fail or never heal. If a point (F, Γ) is above the null curve given by equation (16), the shear stress increases, otherwise it decreases. Similarly, if a point (F, Γ) is to the right of the null curve, $R = 0$, the rock competency decreases. These four cases suggest a classification of fault dynamics: intact stable sliding, failed stable sliding, multiple state, and oscillatory sliding.

In the previous discussion, it is assumed that the shear viscosity is a function of rock competency only. In fact, shear viscosity depends strongly on porosity and grain size distribution, that is, $\mu^* = \mu^*(\Theta)$. Since grain-size distribution, temperature-dependent intrinsic viscosity of minerals, and porosity change, the null curve given by equation (16) can be viewed as an instantaneous function of rock texture. For example, as the grains get smaller due to gouge, the shear viscosity decreases and the stress null curve tends to intersect the S-shape curve ($R = 0$) at lower or higher Γ values depending on the S-shape curve. Similarly, particle size increase due to diagenesis can significantly change the behavior. Thus, gouge and diagenesis can determine which of the modes of fault behavior noted previously are realized for a given fault system.

Failure is a fast process, and healing is a slow one. Therefore, the coefficient k in equation (13) is very large when the (F, Γ) point is to the right of the S-shape curve. On the other hand, for low shear viscosities (low Γ values), it is anticipated that the solution will follow equation (16) rather than the S-shape curve ($R = 0$) because k is small in this region.

Suppose that $\dot{E}$ is large so that the null curves intersect on the lowest branch of the S-shape curve. If such a system experiences a sudden change in $\dot{E}$, it can result in damped oscillations depending on the coefficients k and $G/\mu(\Gamma)$. If $k \gg G/\mu$, the solution follows the $R = 0$ curve.

Let us consider an experiment wherein we make a series of changes in $\dot{E}$ and observe the response of the system according to the present model. The result is a complex series of state, (F, Γ), changes reminiscent of those observed in slip experiments. Consider a scenario in which $\dot{E}$ is taken to be $\dot{E} = 1$ GPa/m.y. (t = 0–100 yr), $\dot{E} = 100$ GPa/m.y. (t = 100–200 yr), $\dot{E} = 50$ GPa/m.y. (t = 200–300 yr), $\dot{E} = 100$ GPa/m.y. (t = 300–400 yr), $\dot{E} = 1$ GPa/m.y. (t = 400–600 yr). Figures 4 and 5 illustrate the effect of sudden changes of $\dot{E}$ on the shear stress and rock competency. The null curves for different values of $\dot{E}$ are shown in Figure 4. As the value of $\dot{E}$ increases, the intersection of the null curves moves right, that is, the new steady state condition has lower rock competency and failure function (higher shear stress). The starting point A is taken to be the steady state solution for $\dot{E} = 1$. When $\dot{E}$ is increased from 1 to 100, the state in the (F, Γ) plane remains above the $\dot{E} = 100$ curve. As noted above, if a state in (F, Γ) plane is above this curve, shear stress increases. As the state (F, Γ) crosses the S-shape curve, the rock competency decreases

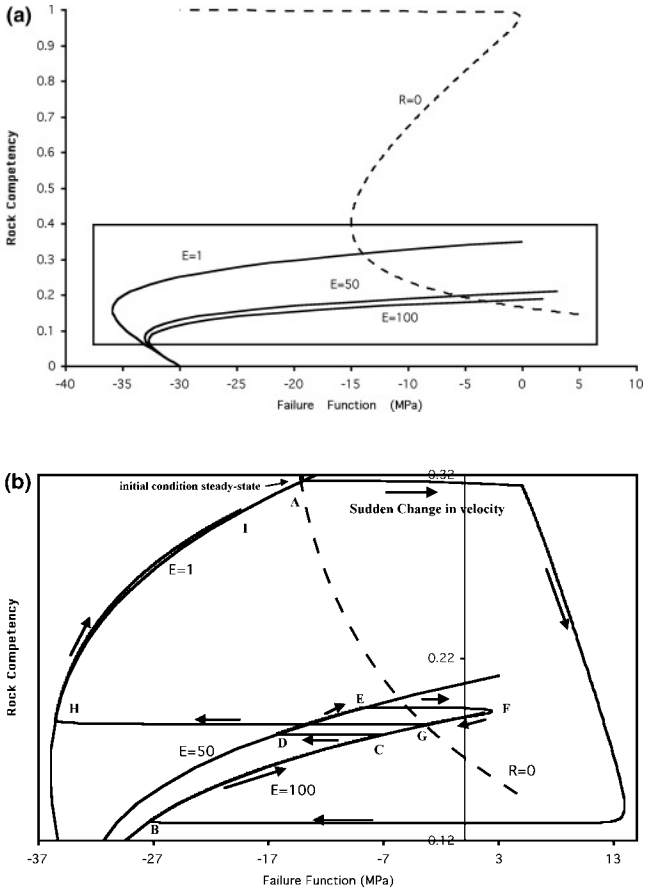

Figure 4. The null curves and phase diagram for a time-dependent $\dot{E}$ (0–100 yr, $\dot{E} = 1$ GPa/m.y.; 100–200 yr, $\dot{E} = 100$ GPa/m.y.: 200–300 years, $\dot{E} = 50$ GPa/m.y.; 300–400 yr, $\dot{E} = 100$ GPa/m.y.; 400–600 yr, $\dot{E} = 1$ GPa/m.y.). The boxed region in Figure a is enlarged in Figure b. The letters and arrows indicate the direction of movement.

since it is now in the $R < 0$ zone. This results in the reduction of cohesion (assumed to be proportional to the rock competency), which in turn increases the failure function. As the rock competency is lost, the shear stress decreases and the failure function increases (state B). Since failure (decrease in rock competency) is a fast phenomenon, the movement from state A to state B is almost instantaneous (Fig. 5). The observed spike in the shear stress follows from equation (9). Failure function is proportional to τ ($F = |\tau| - c$). Therefore, (9) suggests that τ is related to $D\Gamma/Dt$. As failure implies that Γ is a step function in t, then τ should be related to $D\Gamma/Dt$. As the time derivative of a step function is a spike, the spike character of τ follows. From state B to state C, the rock competency increases slowly since healing is a slow process. As $\dot{E}$ is decreased from 100 to 50, a sudden decrease in the shear stress is observed (transition $C \rightarrow D$). However the rock competency remains unchanged corresponding to an almost horizontal trajectory in the F, Γ plane (Fig. 4). Both the rock competency and shear stress increase from state D

to state E. As $\dot{E}$ is increased back to 100, the state crosses the S-shape curve, resulting in a sudden decrease in rock competency and an increase followed by a decrease in shear stress ($E \rightarrow F$). Finally, $\dot{E}$ is reduced to 1 (the initial value), which results in a decrease in the shear stress ($G \rightarrow H$).

As seen in Figures 4 and 5, generally, an increase/decrease in the rate of shear strain results in almost an instantaneous increase/decrease in the shear stress followed by a slow decrease/increase. However, the behavior is shown to be quite complicated if a considerable change in the rock competency is forced as a result of step changes in the shear strain rate (for example the transition $A \rightarrow B$). Another observation is that the time scales of failure ($A \rightarrow B$) and healing ($H \rightarrow I$) are quite different (Fig. 5).

This example demonstrates that even the two variable (F, Γ) model is comprehensive enough to explain many aspects of experimental observations. We should note that in contrast to the state- and rate-dependent friction approach, our starting point is the incremental stress rheology combining poroelasticity and viscosity. Furthermore, our model makes a transition between intact and failed rock states and thereby can be used to analyze fault initiation, growth, branching, and reactivation when placed in the context of a three-dimensional RTM crustal simulator. Another interesting point is that when the x axis of Figure 5b is displayed in log t, the increase in rock competency shows almost a linear variation in log t as observed in experimental studies.

The previous model can support autonomous oscillatory failure reminiscent of the earthquake cycle when the null curves intersect on the unstable (middle) branch. Figure 6 shows the F, Γ plane for an oscillation-supporting set of parameter values ($\dot{E} = 0.06$ GPa/m.y.). The arrows show the direction of movement. Figure 7 illustrates the predicted time dependence of rock competency (Fig. 7a), failure function (Fig. 7b), and shear stress (Fig. 7c). As seen in Figure 7, after a short transient period, the system finds its limit cycle. The stress drop after failure is quite large because of the use of equation (15). It is likely that in two- and three-dimensional simulations, the stress drop will be less due to the interaction of failed and unfailed regions. Furthermore, the frequency of failure events is expected to increase since the energy release at each failure (stress drop) will be less.

While the present two-variable model does display earthquakelike behavior, it does not involve the richness of RTM processes in real fault systems. Furthermore, it would be instructive to integrate a number of the concepts that have been invoked in earthquake modeling as reviewed in the Introduction. We now address such a generalization.

Rock Competency, Fluid Flow, and Compaction Model

Pseudo Three-Dimensional Nine-Variable Model

The two-variable model of the previous section was generalized to investigate the interplay of rock competency,

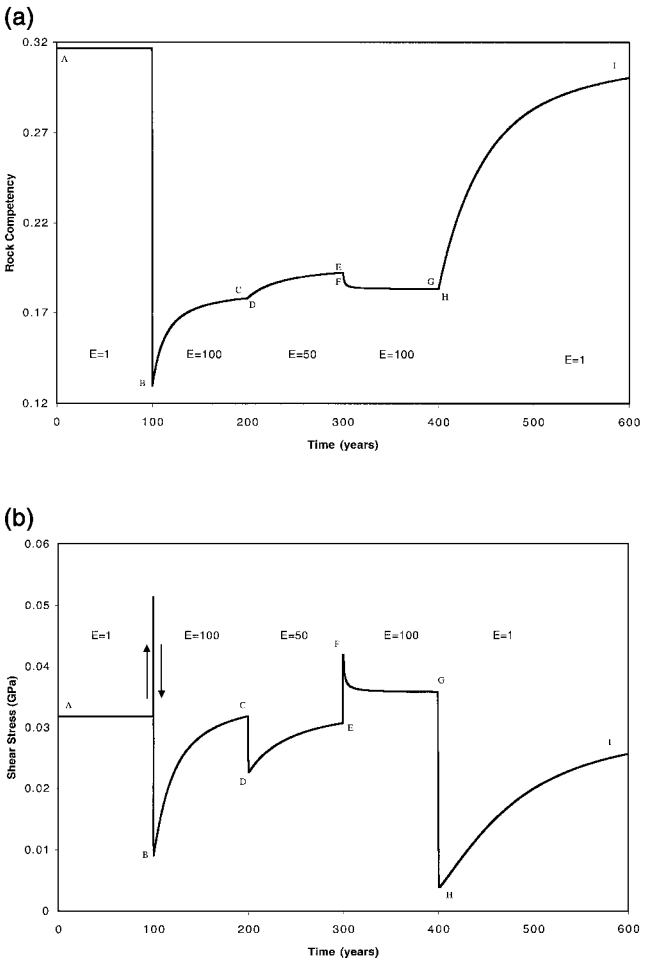

Figure 5. The shear stress and rock competency history for a time-dependent $\dot{E}$ (0–100 yr, $\dot{E} = 1$ GPa/m.y.; 100–200 yr, $\dot{E} = 100$ GPa/m.y.; 200–300 years, $\dot{E} = 50$ GPa/m.y.; 300–400 yr, $\dot{E} = 100$ GPa/m.y.; 400–600 years, $\dot{E} = 1$ GPa/m.y.). The letters indicate the corresponding position in the phase diagram (Fig. 4).

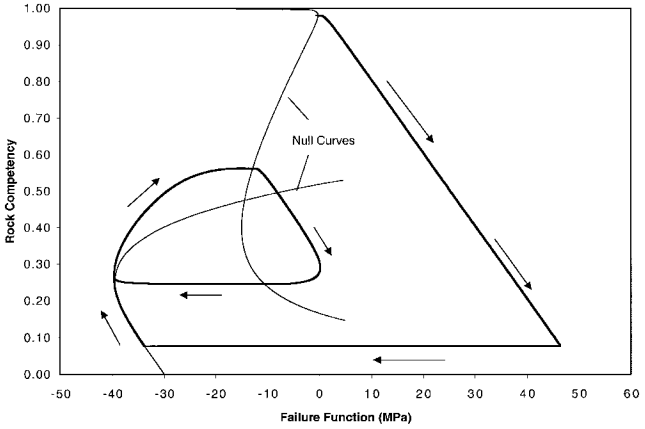

Figure 6. Phase diagram for the oscillatory case (null curves intersect at the unstable branch).

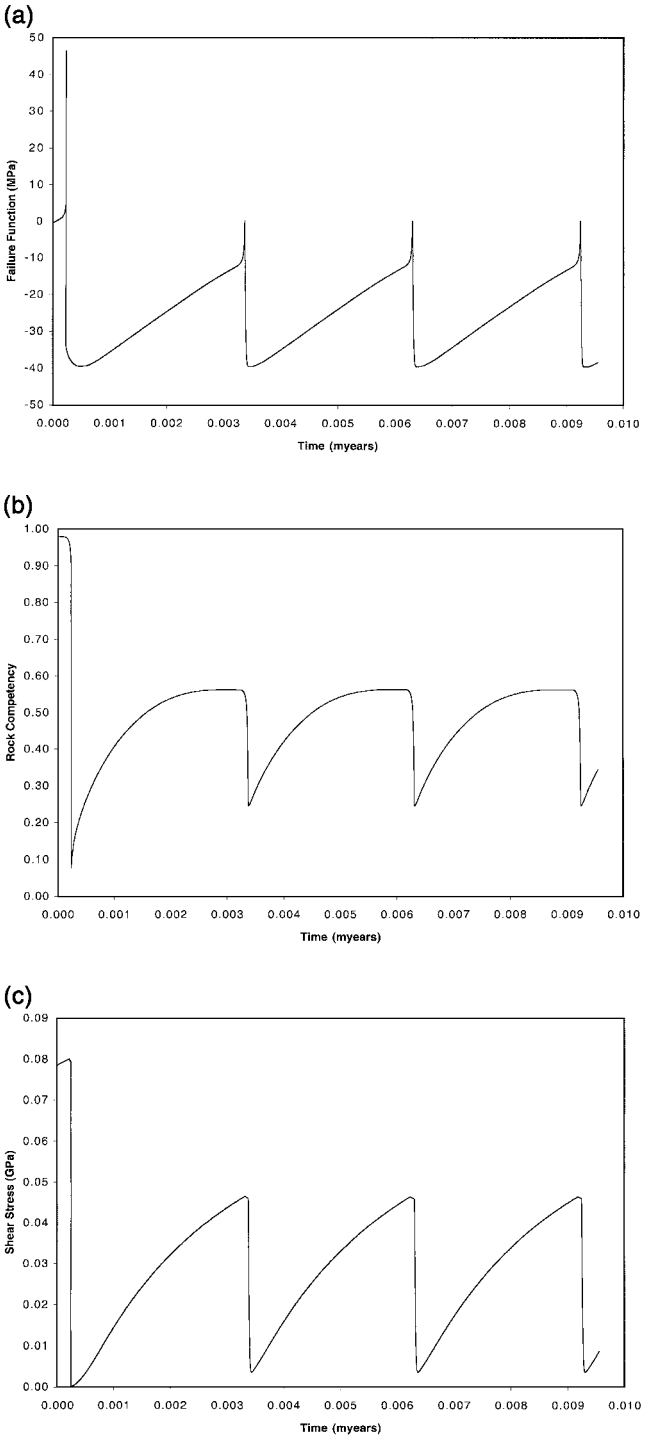

Figure 7. History of (a) rock competency, (b) failure function, and (c) shear stress. After a short transient period, the system finds its limit cycle.

fluid flow, overpressure, and compaction within and around the fault. To do so we also consider the effect of elastic deformation in the country rock, the influence of the width of a fault zone, and the role of fluid pumping from deeper-lying sources. As in our earlier study, we consider a single zone. However, choosing various values of the parameters allows us to contrast zones of continuous slip and those that serve as leading centers of seismic activity. Equations (9) and (14) are generalized to include the fluid pressure, porosity, and other components of the stress tensor.

The conservation of fluid mass equation can be approximated by

$$\phi\beta\bar{\rho}_{\mathrm{f}}\frac{Dp}{Dt} = -\rho_{\mathrm{f}}tr(\dot{\boldsymbol{\varepsilon}}) - A\frac{\kappa\rho_{\mathrm{f}}}{\mu_{\mathrm{f}}w^2}(p - p^*) + B. \quad (17)$$

Here, A is a dimensionless rock property, κ is the permeability of the seal overlying the zone of interest, μ_{f} is the fluid viscosity, β is the fluid compressibility, p^* is the fluid pressure in the zone (above) to which the fluid escapes, w is a characteristic length for pressure dissipation, and B is the fluid influx into the system. The first term on the right-hand side represents volume changes due to deformation. The second term is an approximation for the Darcy flow in or out of the fault system. The last term accounts for the influx ($B > 0$) from a deeper-lying fluid source (Rice, 1992). The permeability is assumed to depend on the rock competency and porosity

$$\kappa = \kappa_0\frac{\phi^3}{\Gamma^2}, \quad (18)$$

where κ_0 is a reference permeability. Here it is assumed that permeability increases as rock competency is lost. Thereby, we include a release mechanism for pressure after failure. The choice of the Γ dependence is made to capture a two order of magnitude increase in permeability as Γ varies over the typical range of competent to failed.

The mass balance equation for the solid phase is

$$\frac{D\phi}{Dt} = (1 - \phi)tr(\dot{\boldsymbol{\varepsilon}}), \quad (19)$$

where it is assumed that the solid grains are incompressible.

The set of equations is completed with the incremental stress rheology

$$\dot{\boldsymbol{\varepsilon}} = \mathbf{C}^{-1}\frac{\mathrm{D}}{\mathrm{Dt}}(\boldsymbol{\sigma} + \alpha p\mathbf{I}) + \boldsymbol{\eta}^{-1}(\boldsymbol{\sigma} + p\mathbf{I}), \quad (20)$$

where $\mathbf{C}$ and $\boldsymbol{\eta}$ are texture-dependent fourth-rank elasticity and viscosity tensors, and α is the effective stress coefficient. We take the x direction as normal to the fault plane and assume that $\dot{\varepsilon}_{yy} = \dot{\sigma}_{zz} = 0$. Equations (19) and (20) naturally couple porosity and stress through the rate of strain. Segall and Rice (1995) proposed an evolution equation for porosity in terms of the slip velocity based on experimental observations. However, they kept the normal stress constant in their numerical treatment. In a three-dimensional fault system, fault width changes to equalize the state of stress in the

country rock and fault zone. Therefore, porosity evolution should be closely related to stress evolution.

We couple this system to the motion of the country rock under the assumption that shear stress in the country rock and fault are equal and the country rock is elastic

$$\frac{D\tau}{Dt} = \frac{G_c}{L_c}(V_c - 2\dot{\varepsilon}_{xy}L_f) \tag{21}$$

where G_c and L_f are the shear modulus of country rock and the half width of the fault, respectively, and V_c is the velocity of the country rock at a distance L_c from the fault. The elastic displacement in the country rock, d, is given by $d = V_c t - 2\varepsilon_{xy}L_f$. Similarly, assuming that the convergence rate of strain at L_c away from the fault is negligible, the following equation can be written to constrain stress and strain normal to the fault:

$$\dot{\sigma}_{xx} = E_c \frac{L_f}{L_c}\dot{\varepsilon}_{xx}, \tag{22}$$

where $E_c = K_c + 413G_c$ and K_c is the bulk modulus of the country rock.

Equations (9), (14), (17), and (19)–(22) are sufficient to determine the nine unknowns Γ, ε_{xx}, ε_{zz}, ε_{xy}, σ_{xx}, σ_{yy}, τ, p, ϕ. To illustrate the effects of various parameters such as fluid influx (the last term in equation 17), shear modulus of country rock, and healing rate, we numerically solve the previous model keeping some of the parameters constant (see Table 1 for system properties and initial conditions). In the following, we consider seven cases. In the first case, the fluid influx rate is taken to be zero, whereas in cases 2 and 3, the fluid influx rate is taken to be 2×10^{-5} g/(cm^3 · yr) and 10^{-5} g/(cm^3 · yr), respectively. In the fourth and fifth cases, the fluid influx rate is assumed to be episodic as suggested by Rice (1992). The importance of healing rate on fault movement is demonstrated in the sixth case. The seventh case is used to illustrate the effect of country rock shear modulus because G_c/L_c is analogous to the spring constant in stick-slip models. The model parameters for these cases are provided in Tables 1 and 2.

Table 1
Model Parameters for All Cases

Shear modulus of country rock (G_c)	200 GPa
Elastic modulus of country rock ($E_c = K_c + 4/3G_c$)	500 GPa
Fault width (2 L_f)	2 m
Country rock influence length (L_c)	1000 m
Velocity of country rock (V_c)	30 m/million yr
Permeability coefficient (κ_0)	1.6×10^{-17} m^2
Compressibility of fluid phase (β)	0.5×10^{-9} Pa^{-1}
Viscosity of fluid phase (μ_f)	0.001 Pa.s
Bulk viscosity of fault rock	20×10^6 GPa yr
Shear viscosity of fault rock (intact rock)	5×10^6 GPa yr
Bulk modulus of fault rock	20 GPa
Shear modulus of fault rock	5 GPa
Vertical stress (σ_{zz})	−150 MPa
Initial normal stress (σ_{xx})	−130 MPa
Initial normal stress (σ_{yy})	−140 MPa
Fluid pressure (p^*)	70 MPa
Initial fluid pressure (p)	70 MPa
Nondimensional coefficient (A in 17)	1.00
Friction angle (φ)	38.65
Cohesion	0
Shear viscosity coefficient (m in $\mu = \mu^*\Gamma^m$)	8.00

Steady Fluid Source and Continuous vs Autonomous Episodic Behavior

The simulated histories of fluid pressure for cases 2 and 3 are shown in Figure 8. The higher value of fluid influx rate results in damped oscillations (case 2), whereas the lower

Table 2
Model Parameters for Different Cases

	B (g/cm^3/yr)	G_c (GPa)	Healing Coefficient (1/MPa yr)
Case 1 (no fluid influx)	0.	200	2.5×10^{-6}
Case 2 (high fluid influx)	2×10^{-5}	200	2.5×10^{-6}
Case 3 (low fluid influx)	10^{-5}	200	2.5×10^{-6}
Case 4 (low freq. fluid influx)	$10^{-5}\left(1 + \cos\left(\frac{2\pi t}{5000}\right)\right)$	200	2.5×10^{-6}
Case 5 (high freq. fluid influx)	$10^{-5}\left(1 + \cos\left(\frac{2\pi t}{2500}\right)\right)$	200	2.5×10^{-6}
Case 6 (high healing rate)	2×10^{-5}	200	1.25×10^{-5}
Case 7 (low shear modulus)	2×10^{-5}	50	2.5×10^{-6}

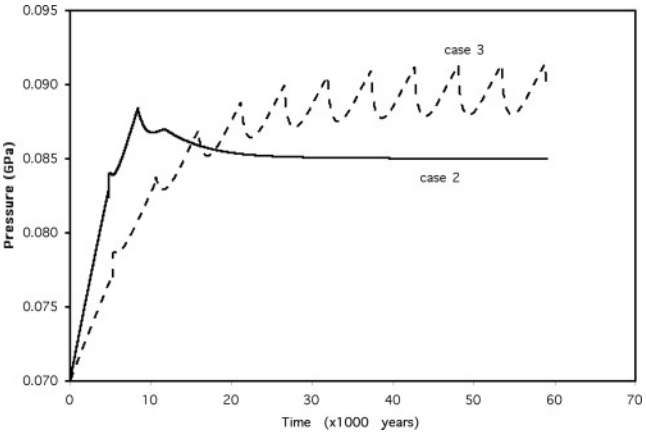

Figure 8. Evolution of fluid pressure for case 2 (high fluid influx rate) and case 3 (low fluid influx rate). The higher value of fluid influx rate results in damped oscillations, whereas the lower fluid influx rate results in sustained oscillations.

fluid influx rate results in sustained oscillations (case 3). The nonoscillatory system gradually approaches a pressure value at which fluid influx is equal to the upward fluid flow since it is assumed that permeability increases with decreasing rock competency (see equation 17). Elevated fluid pressure decreases the effective stress and, as discussed in the previous section, it might result in a more steady behavior. However, Figure 8 shows that the pressure for the lower influx case eventually becomes greater than that for the higher influx rate. This is due to the changes in stress tensor as rock fails. Figure 9 illustrates the evolution of normal stress components σ_{xx} and σ_{yy} for cases 2 and 3. In the oscillatory case, the stress component normal to the fault, σ_{xx}, increases after every rupture event because of the sudden decrease in the shear viscosity as rock competency is lost. This effect tends to widen the fault. Note that in the damped oscillation case, both stress components gradually approach the lithostatic stress σ_{zz}, which is kept constant at 150 MPa. If the strain component normal to the fault was zero, that is, $E_c \to \infty$, then both normal stress components would jump to σ_{zz} after failure. However, since the stress component normal to the fault must be equal to that of country rock (equation 22), σ_{yy} (oscillatory case) shows a quite distinct behavior. After every failure event, σ_{yy} experiences a sudden drop followed by a sudden increase. Note that after failure and sudden drop in the shear stress, the normal stress components approach the principle stresses of the total stress tensor. In summary, σ_{zz} is similar for both cases, but σ_{yy} is more free and more strongly reflects the dynamics of the fault. The time histories of rock competency are shown in Figure 10 for cases 2 and 3. Note that initially the fault system is taken to be competent. A stable sliding state is reached after three failure events for case 2. The first failure events for these cases are at different times because of the relatively high fluid pressure and low rock strength for the high fluid influx rate case. The elastic displacement stored in the country rock as a function of time is shown in Figure 11. In the oscillatory system, the fault slips around 0.15 m approximately every 5000 y. On the other hand, the nonoscillatory system experiences one early major slip. Furthermore, the time scale of the second slip is in the order of hundreds of years. After the second failure event, the stored displacement approaches an equilibrium value at which the shear stress in the country rock is equal to the shear stress required to drive the fault at the low rock competency level shown in Figure 10. The long period of the oscillations is partly due to the large stress drop after failure events. As stress drops get smaller in multidimensional studies, the number of events will increase. Also, the nonuniformity along the fault is likely to decrease the return period of failure events.

Figure 12 compares the shear stress histories for cases 1 (no fluid influx) and 3 (low fluid influx rate) showing that elevated fluid pressure decreases rock strength and results in failure at lower deviatoric stress levels. As seen in the figure, elevated fluid pressure also decreases the period of failure

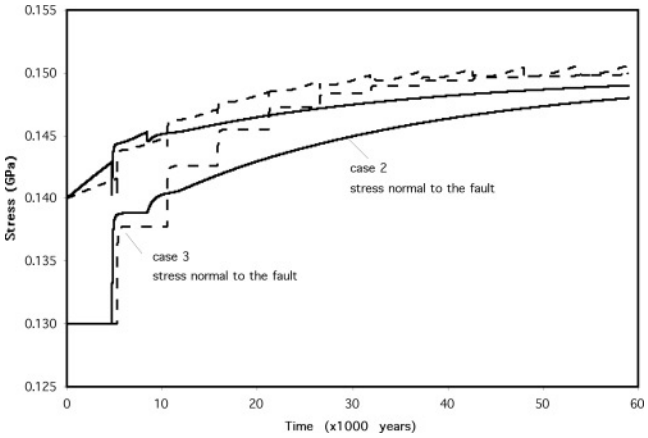

Figure 9. Evolution of σ_{xx} and σ_{yy} for case 2 (high fluid influx rate and case 3 (low fluid influx rate).

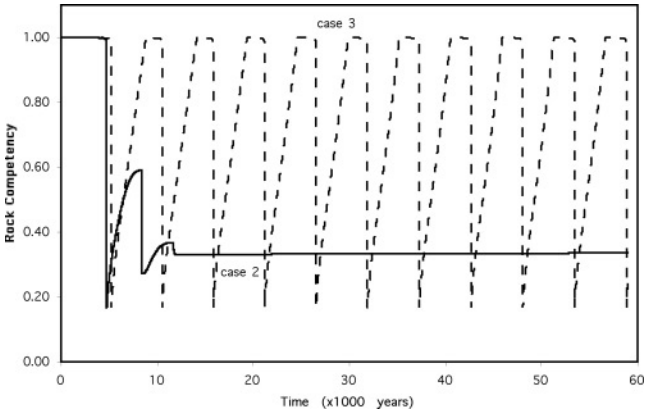

Figure 10. Evolution of rock competency for case 2 (high fluid influx rate) and case 3 (low fluid influx rate). Stable sliding state is reached after three failure events for the higher fluid influx rate case.

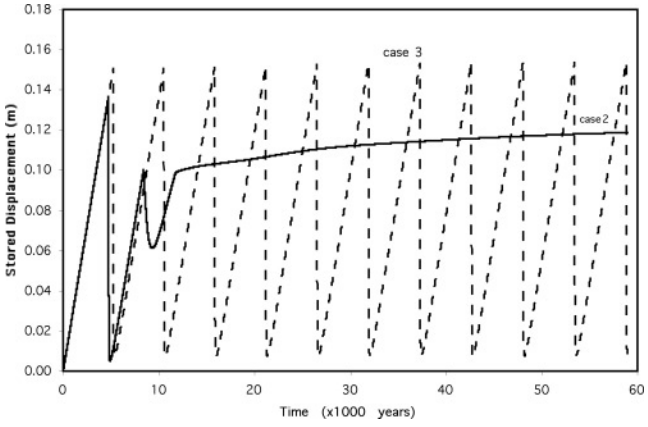

Figure 11. Evolution of elastic displacement stored in the country rock for case 2 (high fluid influx rate) and case 3 (low fluid influx rate). The oscillatory case shows a 0.14 m displacement during every failure event.

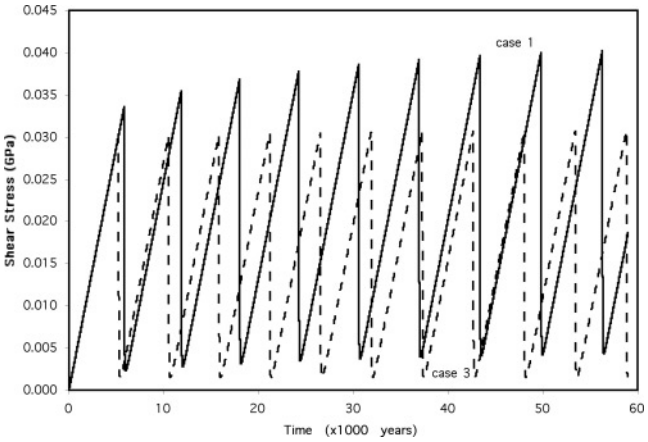

Figure 12. Evolution of shear stress for case 1 (no fluid influx) and case 3 (low fluid influx rate). When there is no fluid influx, the stress drop is greater.

since it decreases the amount of elastic energy that can be stored in the country rock.

Oscillatory Fluid Pumping: Periodic and Chaotic Response

In cases 4 and 5, the fluid influx rate is assumed to be an oscillatory function of time to study the effects of possible episodic influx from deeper zones of a fault system. Both examples of periodic oscillatory pumping result in an oscillatory dynamics. However, the time dependence of the pressure and stress components are quite different as seen in Figures 13 and 14. A comparison between Figure 13 (case 4) and Figure 8 (case 3) shows that the time-dependent fluid influx rate influences the amplitude of pressure oscillations. However, the period of failure does not appreciably change since the period of fluid influx in case 4 is taken to be close to the period of autonomous oscillations in case 3. When the period of fluid influx rate is lowered to 2500 yr, although the number of failure events remains the same, the time dependence of pressure and stress is affected significantly. Case 5 shows that the response to a periodic fluid influx from below can be chaotic in time as suggested in Figure 15a. The object to which the dynamics is attracted in the nine-dimensional space of the descriptive variables is hinted at through its projection in the (F, Γ) plane in Figure 15b. Near $\Gamma = 1$ and along the fall from the upper right toward the lower left, the attraction is thin associated with the short time scale of failure. In going from the lower left to the top ($\Gamma = 1$), the attraction broadens to reveal that in the present model, the conditions at which an event is triggered, the sharp right corner, is predictable, whereas the scenario of healing, and hence the time between event, is more variable. Since porosity, pressure, and stress components are tightly coupled through the mass balance equations of solid and fluid phases and incremental stress rheology, a disturbance in one of the variables is reflected in the other variables. Figure 16 illustrates the response of porosity to the episodic

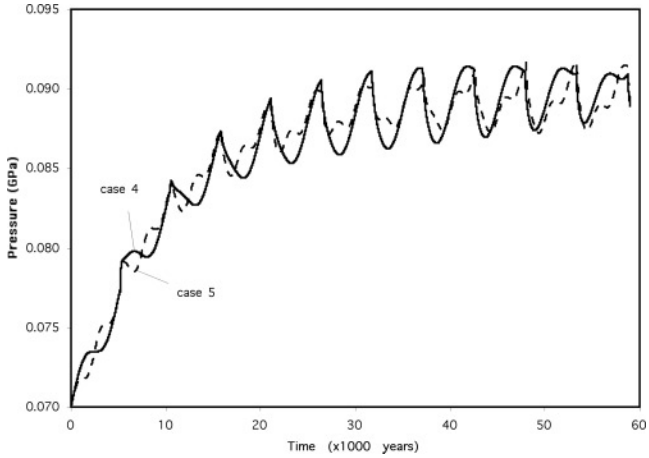

Figure 13. Evolution of fluid pressure for case 4 (low-frequency fluid influx rate) and case 5 (high-frequency fluid influx rate). Increased frequency in the fluid influx rate increases the temporal complexity of fluid pressure.

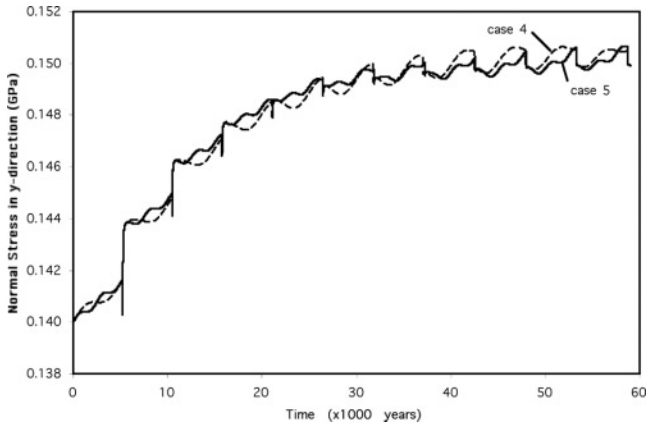

Figure 14. Evolution of σ_{yy} for case 4 (low-frequency fluid influx rate) and case 5 (high-frequency fluid influx rate).

fluid influx. The correlation of Figures 16 and 13 suggests that in this particular simulation, the changes in porosity is mainly due to the elastic response of the fault to pressure variations.

Fault Healing

At great depth or under the influence of a large heat influx from beneath the fault, fluid-rock interactions are fast. In this case, rocks can heal fast once failed, or, in fact, reaction-induced healing can keep in step with failure. If chemical reactions heal the rock (and thereby increase rock competency) are fast, even at large driving forces (large $\dot{E}$ or V_c), it is possible that rock can gain strength, keeping the failure function negative, namely, suppressing failure. Therefore, high healing rate might allow stress to build up, promoting a stick-slip type fault behavior. The term *stick-*

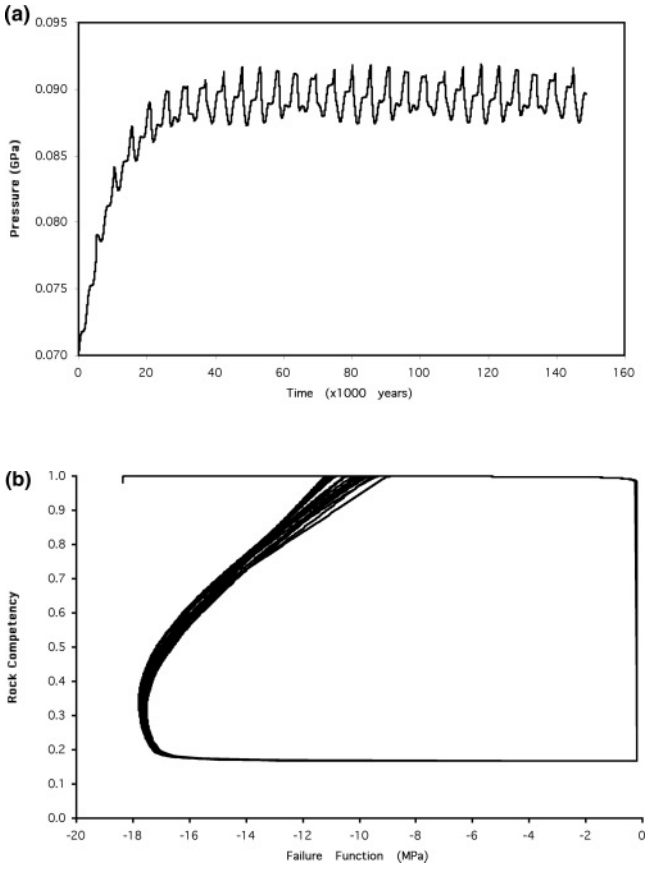

Figure 15. (a) Evolution of fluid pressure (case 5); (b) trajectory on F, Γ plane. Although the trajectories are close to each other, the system does not reach a limit cycle.

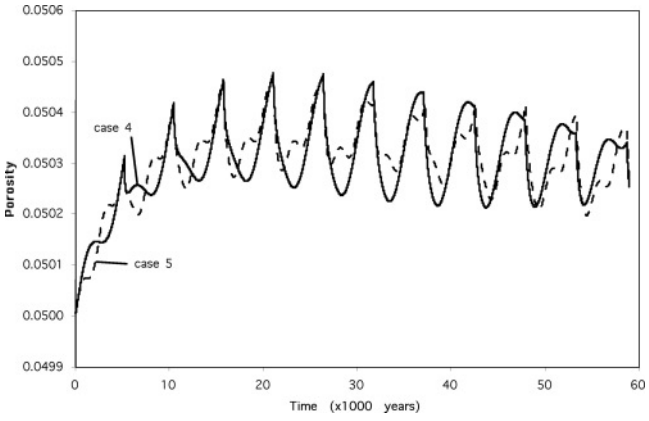

Figure 16. Evolution of porosity for case 4 (low frequency fluid influx rate) and case 5 (high frequency fluid influx rate). Failure is followed by a porosity decrease as a result of loss of fluid pressure due to fracturing.

slip is used in a wider context. It is meant here to include both cyclic jumping between the high and low branches of the *S*-shaped curve and changes in the rock competency at the lower branch of the *S*-shape curve only as discussed earlier. Figure 17 shows the evolution of rock competency for cases 2 (high fluid influx rate) and 6 (high fluid influx and healing rates). As anticipated, faster healing fault systems experience a greater number of failures before reaching steady state. Thus increasing the healing rate can move the fault into the autonomous oscillation regime.

Country Rock Rheology

The country rock shear modulus is another factor that affects both failure frequency and amount of slip, illustrating the classic inverse relation between event frequency and amplitude. As shown in Figure 18, when the country rock shear

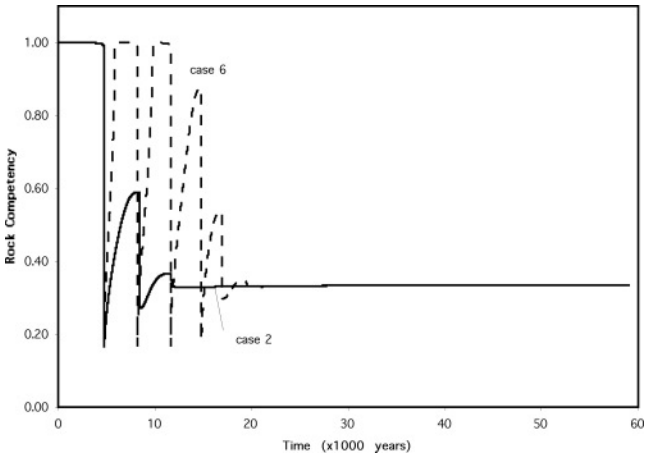

Figure 17. Evolution of rock competency for case 2 (high fluid influx rate) and case 6 (high healing rate). Faster healing system shows a greater number of failures before reaching steady state.

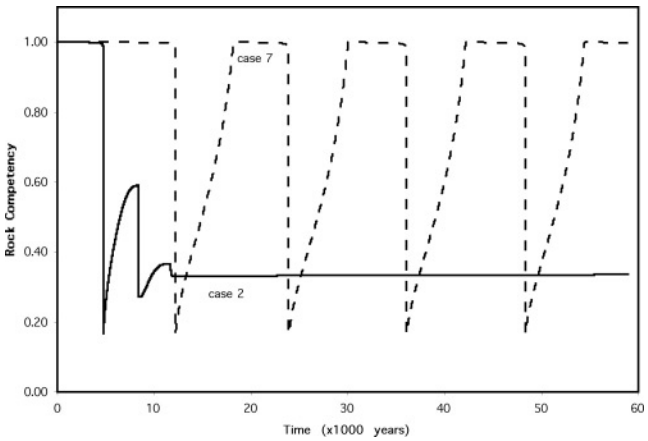

Figure 18. Evolution of rock competency for case 2 (high fluid influx rate) and case 7 (low country rock shear modulus). Low country rock shear modulus tends to result in an oscillatory system.

modulus is lowered (case 7), it may change an nonoscillatory system (case 2) into an oscillatory one. Low shear modulus increases failure period since it takes more time to reach the stress level required to fail the rock. Such a system is likely to have larger slips during a failure event as seen in Figure 18. An investigation of equations (14) and (22) shows that

$$\frac{D\tau}{Dt} = \left[\mu\left(\frac{1}{G_f} + \frac{L_c}{L_f G_c}\right)\right]^{-1}\left[\mu\,\frac{V_c}{L_f} - \tau\right]. \qquad (23)$$

When the shear modulus of the country rock G_c is infinite, the rate coefficient (forefactor) becomes that of equation (14), whereas small values of G_c results in low rate effective coefficients, tending to increase the stored displacement and shear stress after failure as observed in Figures 19 and 20.

Conclusions

We present a model based on incremental stress rheology and rock competency dynamics to study the memory and failure of rocks in a fault zone. The model differs from previous ones as it accounts for the transition from intact to failed rock states. Therefore, it can be used to study the self-organization of fault systems from the intact rock state as well as the response of an active fault system to various external factors (fluid influx or overall plate motion) or internal processes (chemical healing, texture dynamics, or fluid overpressuring) effects. Also the incremental stress rheology used in this study can be generalized to include the rate of strain due to fracturing, pressure solution and gouge (Ortoleva 1994a, 1998; Ozkan *et al.,* 1998; Tuncay *et al.,* 2000a,b). Although some of the functions (such as *S*-shape curve used in the rock competency equation and rock competency dependence of the shear viscosity) are not yet tested experimentally, it has been shown that the present approach can capture the features of slip experiments. Furthermore, since mass and momentum balance equations are employed, pressure, porosity, rate of strain, and stress tensors are consistently coupled.

The richness of the fault system dynamics is illustrated in Figure 15. The fault zone is represented by a set of nine ordinary differential equations and not as a spatially continuous set of partial differential equations as required to capture inner fault structure and overall fault geometry and temporal dynamics. Despite the simplicity of the present nine-variable, single-spatial zone system, the response is exceedingly complex.

As the texture model gets richer, elastic and viscous properties can be more accurately expressed in terms of texture variables, which evolves via the Markov-type differential equations. Clearly, grain size, shape, and number density are not sufficient to characterize rheologic and other properties. Our motion of rock competency as the fraction of grain–grain contacts is just an important step in developing a sufficiently comprehensive texture model.

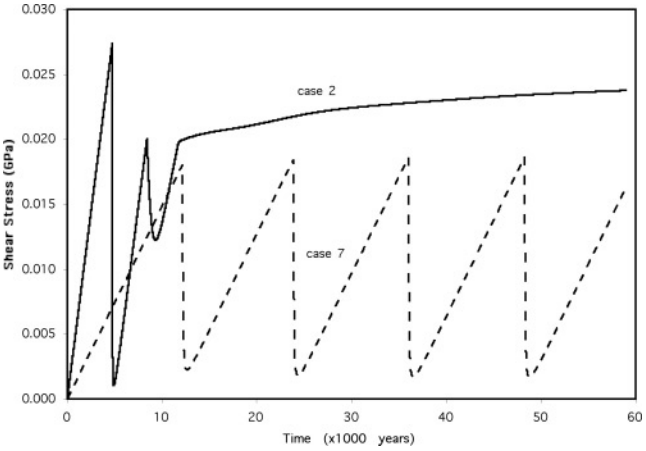

Figure 19. Evolution of shear stress for case 2 (high fluid influx rate) and case 7 (low country rock shear modulus). Low country rock shear modulus is seen to increase the stored displacement.

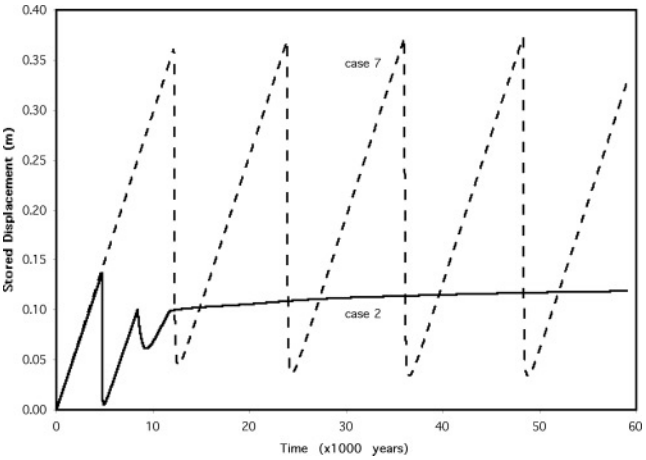

Figure 20. Evolution of elastic displacement stored in the country rock for case 2 (high fluid influx rate) and case 7 (low country rock shear modulus). Low country rock shear modulus is seen to increase the stress drop.

Fault mechanics modeling must be carried out in three spatial dimensions and via a model that incorporates a full suite of crustal RTM processes. In earlier studies (Ortoleva 1994a, 1998; Ozkan *et al.,* 1998; Tuncay *et al.,* 2000a,b), we showed how this can be accomplished and presented results as applied to sedimentary basins. We believe that the present model, as applied to competency, fluid flow, diagenesis and deformation in each macrovolume element of a finite-element approach will allow for first principles fault simulation. As our model accounts for the full range of rock states (intact to failed), a three-dimensional finite-element approach will allow for the prediction of fault morphology (thickness, overall shape, branching) as well as reactivation of healed sections of a previously active zone.

Acknowledgments

This work was supported by a contract with the Gas Research Institute and the Office of Sciences of the U.S. Department of Energy. We would like to thank Dr. F. Renard (Oslo University) and Professor H. Al-Shukri (University of Arkansas) for stimulating discussions on the conceptual model.

References

Berryman, J. G. (1980). Long-wavelength propagation in composite elastic media. I. Spherical inclusions, *J. Acoust. Soc. Am.* **68,** 1809–1819.

Berryman, J. G. (1986). Effective medium approximation for elastic constants of porous solids with microscopic heterogeneity, *J. Appl. Phys.* **59,** 1136–1140.

Blanpied, M. L., D. A. Lockner, and J. D. Byerlee (1995). Frictional slip of granite at hydrothermal conditions, *J. Geophys. Res.* **100,** 13,045–13,064.

Brace, W. F., and J. D. Byerlee (1966). Stick-slip as a mechanism for earthquakes, *Science* **153,** 990–992.

Byerlee, J. D. (1990). Friction, overpressure and fault normal compression, *Geophys. Res. Lett.* **17,** 2109–2112.

Chester, F. M. (1994). Effects of temperature on friction: constitutive equations and experiments with quartz gouge, *J. Geophys. Res.* **99,** 7247–7261.

Chester, F. M. (1995). A rheologic model for wet crust applied to strike-slip faults, *J. Geophys. Res.* **100,** 13,033–13,044.

Desai, C. S., and H. J. Siriwardane (1984). *Constitutive Laws for Engineering Materials,* Prentice-Hall, Inc., Englewoods Cliffs, New Jersey.

Dewers, T., and P. Ortoleva (1994). Nonlinear dynamical aspects of deep basin hydrology: fluid compartment formation and episodic fluid release, *Am. J. Sci.* **294,** 713–755.

Dieterich, J. H. (1978). Time-dependent friction and the mechanics of stick-slip, *Pure Appl. Geophys.* **116,** 790–806.

Dieterich, J. H. (1979). Modeling of rock friction. Experimental results and constitutive equations, *J. Geophys. Res.* **84,** 2161–2168.

Drüker-Prager, D. C., and W. Prager. (1952). Soil mechanics and plastic analysis or limit design, *Quarterly of Applied Mathematics* **10,** 157–165.

Fournier, R. O. (1996). Compressive and tensile failures at high fluid pressure where preexisting fractures have cohesive strength, with application to the San Andreas Fault. *J. Geophys. Res.* **101,** 25,499–25,509.

Fredrich, J. T., and B. Evans (1992). Strength recovery along simulated faults by solution transfer processes. In *33rd U.S. Rock Mechanics Symposium,* J. R. Tillerson and W. R. Warersik, (Editors), Balkema, Rotterdam, 121–130.

Henderson, J. R., and B. Maillot. (1997). The influence of fluid flow in fault zones on patterns of seismicity: a numerical investigation, *J. Geophys. Res.* **102,** 2915–2924.

Hickman, S., R. Sibson, and R. Bruhn. (1995). Introduction to the special issue: mechanical involvement of fluid in faulting, *J. Geophys. Res.* **100,** 12,831–12,840.

Lachenbruch, A. H. (1980). Frictional heating, fluid pressure and the resistance to fault motion, *J. Geophys. Res.* **85,** 6097–6112.

Lee, T.-C. 1996. Pore-pressure rise, frictional strength, and fault slip: one-dimensional interaction models. *Geophys. J. Int.* **125,** 371–384.

Linker, M. F., and J. H. Dieterich. 1992. Effects of variable normal stress on rock friction: observations and constitutive relations, *J. Geophys. Res.* **97,** 4923–4940.

Lockner, D. A., and J. D. Byerlee. (1994). Dilatancy in hydraulically isolated faults and the suppression of instability, *Geophys. Res. Lett.* **21,** 2353–2356.

Lockner, D. A., and J. D. Byerlee. (1995). An earthquake instability model based on faults containing high fluid-pressure compartments, *Pure Appl. Geophys.* **145,** 717–745.

Logan, J. M., and L. W. Teufel, (1986). The effect of normal stress on the real area of contact during frictional sliding of rocks, *Pure Appl. Geophys.* **124,** 471–486.

Marone, C., C. H. Scholz, and R. Bilham, (1990). Frictional behavior and constitutive modeling of simulated fault gouge, *J. Geophys. Res.* **95,** 7007–7025.

Matthai, S. K., and G. Fischer (1996). Quantitative modeling of fault-fluid-discharge and fault-dilation-induced fluid-pressure variations in the seismogenic zone, *Geology* **24,** 183–186.

Miller, S. A., A. Nur, and D. L. Olgaard. (1996). Earthquakes as a coupled stress: high pore pressure dynamical system, *Geophys. Res. Lett.* **23,** 197–200.

Morrow, C. A., and J. D. Byerlee. (1989). Experimental studies of compaction and dilatancy during frictional sliding on faults containing gouge, *J. Struct. Geol.* **11,** 815–825.

Ortoleva, P., (Editor) (1990). Self-organization in geological systems, *Earth-Science Reviews* **29,** 1–4.

Ortoleva, P. (1992). Nonlinear Chemical Waves, Wiley, New York.

Ortoleva, P. (1994a). Geochemical Self-Organization, Oxford University Press, Oxford, U.K.

Ortoleva, P. (Editor) (1994b). Basin compartmentation: definitions and mechanisms, in *Basin Compartments and Seals,* AAPG Memoir 61, 39–52.

Ortoleva, P. (1998). *Basin Compartment Fundamentals,* GRI Topical Report, Contract No. GRI-97/0097, Gas Research Institute, Chicago.

Ortoleva, P., J. M. Maxwell, D. Payne, W. Sibo, and J. Comer (1997). Naturally fractured reservoirs and compartments: a predictive basin modeling approach, in *Fractured Reservoirs: Characterization and Modeling,* T. E. Hoak, A. L. Klawitter, and P. K. Blomquist (Editors), Rock Mountain Association of Geologists Guidebook, Rocky Mountain Association of Geologists, Denver, 67–102.

Ozkan, G., and P. Ortoleva (2000). Evolution of gouge grain size distribution: a Markov model, *Pure Appl. Geophys.* **157,** 449–468.

Ozkan, G., K. Tuncay, and P. Ortoleva (1998) Process-based fault seal/conduit prediction, in *1998 AAPG Annual Convention Abstracts* (CD-ROM format), Salt Lake City, Utah, 17–28 May 1998.

Renard, F., and P. Ortoleva (2001). *Memory and the Self-Organizing Planet* (forthcoming).

Rice, J. R. (1992). Fault stress states, pore pressure distributions, and the weakness of the San Andreas Fault, in *Fault Mechanics and Transport Properties in Rocks,* B. Evans and T.-F. Wong (Editors), Academic Press, London, 475–503.

Rice, J. R., and J. C. Gu (1983). Earthquake aftereffects and triggered seismic phenomena, *Pure Appl. Geophys.* **121,** 187–219.

Rice, J. R., and A. Ruina (1983). Stability of steady frictional slipping, *J. Appl. Mech.* **50,** 343–349.

Rudnicki, J. W., and C.-H. Chen (1988). Stabilization of rapid frictional slip on a weakening fault by dilatant hardening, *J. Geophys. Res.* **93,** 4745–4757.

Ruina, A. (1983). Slip instability and state variable friction laws, *J. Geophys. Res.* **88,** 10,359–10,370.

Scholz, C. H. (1990). *The Mechanics of Earthquakes and Faulting,* Cambridge University Press, New York.

Scholz, C. H. (1992). Paradigms or small changes in earthquake mechanics, in *Fault Mechanics and Transport Properties in Rocks,* B. Evans and T.-F. Wong (Editors) Academic Press, London, 505–517.

Segall, P., and J. R. Rice (1995). Dilatancy, compaction, and slip instability of a fluid-infiltrated fault. *J. Geophys. Res.* **100,** 22,155–22,171.

Sleep, N. H. (1995a). Ductile creep, compaction, and rate dependent friction within major fault zones, *J. Geophys. Res.* **100,** 13,065–13,080.

Sleep, N. H. (1995b). Frictional heating and the stability of rate and state dependent frictional sliding, *Geophys. Res. Lett.* **22,** 2785–2788.

Sleep, N. H. (1997). Application of a unified rate and state friction theory to the mechanics of fault zones with strain localization. *J. Geophys. Res.* **102,** 2875–2895.

Sleep, N. H., and M. L. Blanpied (1994). Ductile creep and compaction: a mechanism for transiently increasing fluid pressure in mostly sealed fault zones, *Pure Appl. Geophys.* **143,** 9–40.

Tse, S. T., and J. R. Rice (1986). Crustal earthquake instability in relation to the depth variation of frictional slip properties, *J. Geophys. Res.* **91,** 9452–9472.

Tullis, T. E. (1988). Rock friction constitutive behavior from laboratory experiments and its implications for an earthquake prediction field monitoring program, *Pure Appl. Geophys.* **126,** 555–588.

Tuncay, K., A. Park, and P. Ortoleva (2000a). A forward model of three dimensional fracture orientation and characteristics, *J. Geophys. Res.* **105,** 16,719–16,735.

Tuncay, K., A. Park, and P. Ortoleva (2000b). Sedimentary basin deformation: an incremental stress rheology approach, *Tectonophysics* **323,** 77–104.

Tuncay, K., and P. Ortoleva (2001). Salt tectonics as a self-organizing process: a three dimensional reaction, transport and mechanics model. *J. Geophys. Res.* **106,** 803–818.

Yamashita, T. (1997). Mechanical effect of fluid migration on the complexity of seismicity, *J. Geophys. Res.* **102,** 17,797–17,806.

Yamashita, T. (1998). Simulation of seismicity due to fluid migration in a fault zone, *Geophys. J. Int.* **132,** 674–686.

Laboratory for Computational Geodynamics
Chemistry Building
Indiana University
Bloomington, Indiana, 47405
ktuncay@indiana.edu
ortoleva@indiana.edu

Manuscript received 9 September 1999.